Available online at www.sciencedirect.com
ScienceDirect
Solid State Ionics 178 (2007) 77–82
SOLID STATE IONICS
www.elsevier.com/locate/ssi

Neutron powder diffraction study at high temperature of the Ruddlesden–Popper phase $Sr_3Fe_2O_{6+\delta}$

F. Prado [a,*], L. Mogni [a], G.J. Cuello [b], A. Caneiro [a]

[a] Centro Atómico Bariloche, CNEA, S. C. de Bariloche 8400, Argentina
[b] Institut Laue-Langevin, BP 156, F-38042 Grenoble Cedex 9, France

Received 22 May 2006; received in revised form 1 September 2006; accepted 25 November 2006

Abstract

The crystal and oxygen defect structure of the $n=2$ Ruddlesden–Popper phase $Sr_3Fe_2O_{6+\delta}$ have been studied by *in situ* high temperature neutron powder diffraction in the temperature range $20 \le T \le 900$ °C in air. The analysis of the neutron diffraction data revealed the presence of structural oxygen vacancies on both the O(1) sites linking the octahedra along the *c* axis and the O(3) sites in the FeO_2 planes of the perovskite layers. The oxygen vacancies on the O(3) site increase with temperature up to ~ 0.25 per formula unit at $T=900$ °C. This result supports previously proposed oxygen ion diffusion mechanism in $Sr_3Fe_2O_{6+\delta}$ that involves the migration of vacancies from an O(3) site to an adjacent O(1) site. The total linear expansion along the *c* axis $\alpha_c = 17.7(5) \cdot 10^{-6}\ K^{-1}$ mainly affects the perovskite block while the width of the rock salt layers remains stable with temperature. The total volumetric expansion $\alpha_V / 3 = 20(1) \cdot 10^{-6}\ K^{-1}$ is around the average of the TEC values (14.8–27.1 K^{-1}) reported for the perovskite system $La_{1-x}Sr_xCo_{1-y}Fe_yO_{3-\delta}$.

Keywords: Mixed conductor oxides; $Sr_3Fe_2O_{6+\delta}$; Ruddlesden–Popper phases; Oxygen defects; Ionic conductivity

1. Introduction

Metal oxides exhibiting mixed oxide-ion and electronic conduction at high temperature have been extensively investigated as potential candidates to be used in electrochemical applications such as electrodes in solid oxide fuel cell, oxygen separation membranes and methane conversion reactors [1–3].

Large ionic conductivity (σ_i) values were reported for the perovskite phases $La_{1-x}Sr_xCo_{1-y}Fe_yO_3$ by Teraoka et al. [4,5]. They found that σ_i rises with increasing Sr and Co content because of the increasing oxygen vacancy concentration, which improves the oxide-ion mobility. Unfortunately, large concentration of oxygen vacancies induces structural transformations to ordered structures due to the interactions among oxygen defects [6–9].

The search for new oxides with mixed conductivity and better structural stability than the perovskite phases have stimulated the exploration of the high temperature properties of materials with perovskite-related intergrowth crystal structures such as the Ruddlesden–Popper [10] series of oxides $(La,Sr)_{n+1}(Fe,Co)_nO_{3n+1}$ [11–14]. The crystal structure of the $n=2$ member of the R–P series, $Sr_3Fe_2O_{6+\delta}$, is tetragonal (S.G. *I4/mmm*) and consists of two $SrFeO_3$ perovskite layers alternating with SrO rock salt layers stacked along the *c* axis [15]. The oxygen atoms are located at three different crystallographic sites, the O(1) site connecting the octahedra along the *c* axis, the O(2) site in the rock salt layer and the O(3) site located in the FeO_2 layers (see Fig. 1). The oxygen content of this compound varies from 6.00 at $T \sim 1000$ °C and $pO_2 \sim 10^{-5}$ atm [15,16] to 7.00 when the sample is heat treated at $T=500$ °C under an oxygen pressure of $P=500$ atm [15]. The ionic conductivity of $Sr_3Fe_2O_{6+\delta}$ was estimated to be $\sigma_i = 1.5 \cdot 10^{-2}\ S\ cm^{-1}$ at $T=900$ °C by means of oxygen permeation measurements [12]. This value is lower than those values reported for the perovskite phases rich in Sr and Co ($\sigma_i \le 1\ S\ cm^{-1}$) but similar to other perovskite phases containing La in the A site [12]. Attempts to improve the oxide-ion conduction in the $n=2$ R–P phase $Sr_3Fe_2O_{6+\delta}$ involved the partial substitution of Fe by other transition metals such as Ti [17], Co [12] or Ni [18,19]. It was

* Corresponding author. Tel.: +54 2944 445288; fax: +54 2944 445299.
E-mail address: fprado@cab.cnea.gov.ar (F. Prado).

0167-2738/$ - see front matter © 2006 Elsevier B.V. All rights reserved.
doi:10.1016/j.ssi.2006.11.014

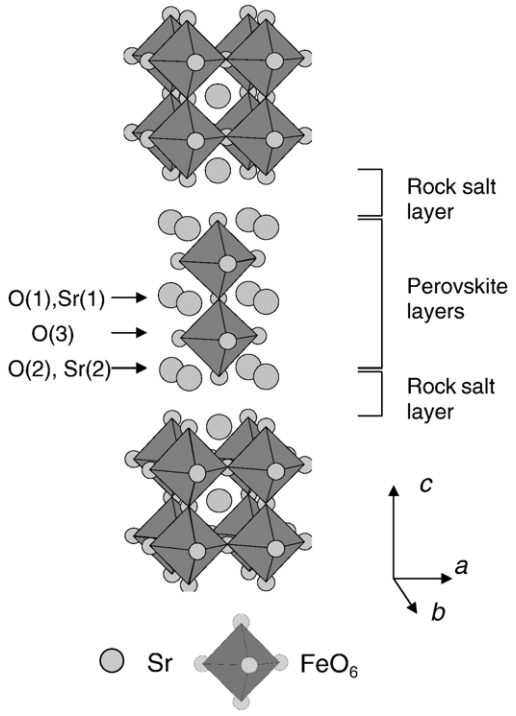

Fig. 1. Crystal structure of $Sr_3Fe_2O_{6+\delta}$.

found that σ_i decreases with the substitution of $Fe^{3+/4+}$ for Ti^{4+}, while increases with the substitution of $Fe^{3+/4+}$ for $Co^{3+/4+}$ or $Ni^{3+/4+}$. At the same time the oxygen vacancy concentration increases for the Co- and Ni-containing samples [12,18] and decreases for those samples doped with Ti [17]. When the oxide-ion diffusion occurs via a vacancy mechanism, σ_i varies with the oxygen vacancy concentration of the material. In order to understand the oxygen diffusion mechanism in $Sr_3Fe_2O_{6+\delta}$, it is essential to determine the oxygen defect structure at high temperature. Recently we proposed a simple defect model for $Sr_3Fe_2O_{6+\delta}$ [16] assuming oxygen vacancies located on the O (1) and O(3) sites to reproduce thermodynamic data. This assumption was in agreement with a previous work of Shilova et al. [17], in which the authors proposed an oxygen diffusion mechanism involving oxygen jumps from the filled O(3) site to an empty O(1) position. Previous analysis of neutron powder diffraction data on samples of $Sr_3(Fe,Co)_2O_{7-\delta}$ quenched from high temperature to control the oxygen content between 6 and 7 [15,20] located the oxygen vacancies only on the O(1) site.

To investigate the crystal chemistry of $Sr_3Fe_2O_{6+\delta}$ at high temperature, we have carried out *in situ* neutron powder diffraction (NPD) measurements in the temperature range $20 \le T \le 900$ °C in air. The analysis of these data led us to determine the behavior of the crystal and oxygen defect structure at high temperature.

2. Experimental

The $Sr_3Fe_2O_{6+\delta}$ sample was prepared by an acetic acid based gel route using $SrCO_3$ (99.99%) and $Fe(CH_3COO)_2 \cdot xH_2O$ (99.9% GFS Chemicals) as raw materials. The water content in the acetate was determined by TGA prior to the synthesis. Stoichiometric amounts of the raw materials were dissolved in acetic acid and refluxed at $T=80$ °C for approximately 2 h until a clear solution was obtained. The solution was then heated in a hot plate to obtain a reddish transparent gel, which in turn was dried, decomposed at $T \sim 400$ °C during 30′ and heat treated at 900 °C in air for 24 h. Then, the powder was pressed into 12.7 mm discs and heat treated at $T=1300$ °C for 24 h under flowing oxygen. After that, the sample was cooled down to room temperature at a rate of 1 °C/min with an intermediate heat treatment at $T=400$ °C for 12 h to maximize the oxygen content of the phase. The final product was stored in a vacuum chamber or in a sealed glass tube under vacuum at room temperature to prevent the degradation of the $Sr_3Fe_2O_{6+\delta}$ phase with atmospheric water at room temperature [12,21]. The sample was characterized by X-ray diffraction with a Philips PW 1700 diffractometer using Cu Kα radiation and a graphite monochromator. The X-ray powder diffraction pattern of the $Sr_3Fe_2O_{6+\delta}$ sample indicated that the sample was single phase. All the reflection peaks were indexed according to the tetragonal unit cell (S.G. *I4/mmm*) previously reported for this compound [15]. The homogeneity of the sample was confirmed by SEM observations and EDS analysis.

The neutron diffraction experiments were carried out in Grenoble at the Institute Lau-Langevin on the D2B ($\lambda=1.594$ Å and $5 \le 2\theta \le 150°$) powder diffractometer at $T=20$, 300, 500, 700 and 900 °C in air. The high-resolution of this two-axis diffractometer allows a precise determination of the positions and occupation numbers of oxygen atoms. At room temperature, the sample was handled under flowing He and placed in a vanadium can. For NPD measurements at $T \ge 300$ °C, a quartz tube open at the top was used as sample holder. The NPD data were analyzed by the Rietveld method using the FullProf Program [22]. During the refinements a TCH pseudo-Voigt function was used for the peak shape [23]. The background of the NPD data obtained at $T=20$ °C was refined with a polynomial function, while a linear interpolation of N selected points was used at $T \ge 300$ °C when the quartz tube was used as sample holder. The cell parameters, atomic positions, oxygen sites occupancies, and isotropic thermal parameters were modified during the refinement of the crystal structure. The refinement results were verified by using at least two different sets of initial values for the thermal parameters to avoid a false minimum due to correlation effects between thermal parameters and occupancy.

3. Results and discussion

The evolution with temperature of the crystal structure of $Sr_3Fe_2O_{6+\delta}$ was studied with the Rietveld method [22] by analyzing the NPD data recorded in air in the temperature range $20 \le T \le 900$ °C. As expected, the crystal structure was refined systematically on the basis of the tetragonal space group *I4/mmm* [15]. In Fig. 2a and b we show the NPD data, calculated profile, and the difference between them at $T=20$ °C and $T=900$ °C, respectively. In these figures are also included the position of the allowed reflections for the tetragonal phase. The final structural parameters at 20 and 900 °C are listed in Tables 1 and 2, respectively. Selected bond lengths for all the temperatures are listed in Table 3.

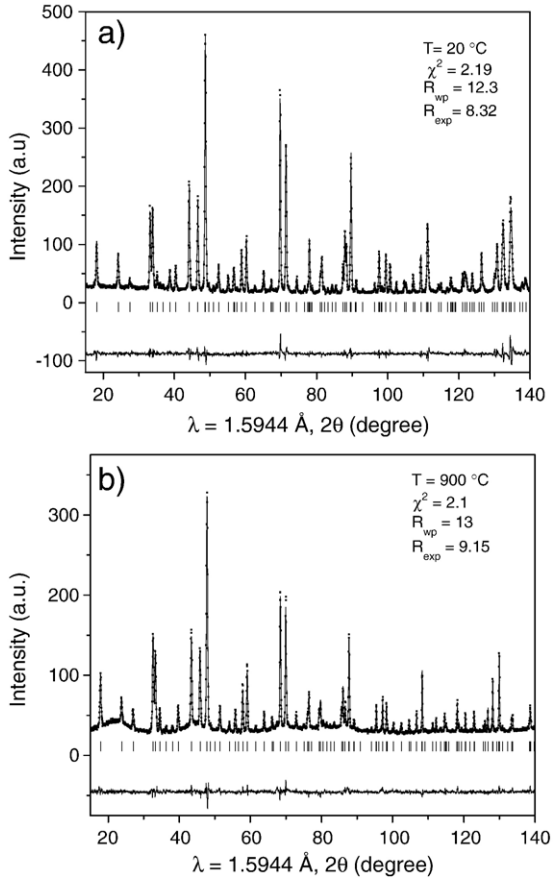

Fig. 2. Observed (D2B), calculated and difference neutron diffraction profiles of $Sr_3Fe_2O_{6+\delta}$ at room temperature (below) and T=900 °C (above) in air. The reflection positions are marked.

The variations of the lattice parameters a and c and the volume V of the tetragonal unit cell with temperature in air are shown in Fig. 3. The lattice parameters expand with increasing temperature. The curves a vs. T and c vs. T exhibit a slope change at T=300 °C, which agrees with the temperature where $Sr_3Fe_2O_{6+\delta}$ begins to lose oxygen [12]. The total expansion coefficients were calculated using the relation,

$$\alpha_p^{\mathrm{Tot}} = \left.\frac{(p-p_0)}{p_0 \Delta T}\right|_{pO_2=\mathrm{cte}} \quad (1)$$

where p stands for the lattice parameters a, c and the unit cell volume V, p_0 represents the values of the lattice parameters and the unit cell volume V at the reference state, and $\Delta T = T - T_0$ stands for the temperature range. The reference state was chosen at T_0=20 °C. The total expansion includes the thermal expansion, defined at constant oxygen content, and the chemical expansion, defined at constant temperature [9]. The total expansion coefficient values calculated from Eq. (1) for the temperature range $20 \le T \le 900$ °C are $\alpha_a = 20.6(8) \cdot 10^{-6}\ K^{-1}$, $\alpha_c = 17.7(5) \cdot 10^{-6}\ K^{-1}$ and $\alpha_V = 60(2) \cdot 10^{-6}\ K^{-1}$. The lower value of α_c compared to α_a is related with the effect of the removal of oxygen atoms from the crystal structure on the lattice parameters. For instance, the chemical expansion of the lattice parameters a and c was examined by *in situ* XRD measurements at T=900 °C in the pO_2 range $10^{-5} \le pO_2 \le 1$ atm. [12]. During these measurements, the lattice parameter a increases while decreasing the pO_2 which indicates the expansion of the Fe–O bond length in the x–y plane. On the contrary, the lattice parameter c diminishes from 20.41 to 20.30 Å when the pO_2 decreases from air to 10^{-5} atm [12]. This behavior is similar to that reported by Weller et al. [15] for samples of $Sr_3Fe_2O_{6+\delta}$ with $0 \le \delta \le 1$ studied by NPD at room temperature. The value $\alpha_V/3 = 20 \cdot 10^{-6}\ K^{-1}$ is higher than the TEC reported for the n=2 R–P phase $Sr_{2.7}La_{0.3}Fe_2O_{6+\delta}$ ($17.4 \cdot 10^{-6}\ K^{-1}$) [24]. The reduction of the total expansion coefficient with increasing La content was attributed to the less ionic La^{3+}–O bond compared to the Sr^{2+}–O bond [24]. Moreover, $\alpha_V/3$ is around the average TEC values (14.8–27.1 K^{-1}) reported for the perovskite system $La_{1-x}Sr_xCo_{1-y}Fe_yO_{3-\delta}$ with $0 \le y \le 1$ and $0 \le x \le 1$ [25].

During NPD measurements, the oxygen content of $Sr_3Fe_2O_{6+\delta}$ was fixed by the oxygen activity of air ($pO_2 \sim 0.209$ atm) and the temperature of the system. The total oxygen content at each temperature was determined by the refinement of the occupancy of the three oxygen crystal sites. At room temperature the total oxygen content was $6+\delta = 6.69(3)$. This value is in good

Table 1
Structural parameters of $Sr_3Fe_2O_{6+\delta}$ at 20 °C [a]

Atom	Site	x	y	z	B_{iso} (Å^2)	Occupancy
Sr(1)	2b	0	0	1/2	0.85(5)	1
Sr(2)	4e	0	0	0.3175(1)	0.83(4)	1
Fe	4e	0	0	0.0987(1)	0.66(3)	1
O(1)	2a	0	0	0	0.8(1)	0.735(8)
O(2)	4e	0	0	0.1940(1)	1.11(4)	1
O(3)	8g	0	1/2	0.0926(1)	0.98(4)	0.990(4)

R_{wp}=12.3%, χ^2=2.191, Dw=0.9.
[a] Space group *I4/mmm*; $a=b$=3.8637(1) Å, c=20.1464(2) Å, V=300.747(2) Å^3.

Table 2
Structural parameters of $Sr_3Fe_2O_{6+\delta}$ at 900 °C [a]

Atom	Site	x	y	z	B_{iso} (Å^2)	Occupancy
Sr(1)	2b	0	0	1/2	2.53(6)	1
Sr(2)	4e	0	0	0.3175(2)	2.52(5)	1
Fe	4e	0	0	0.1011(1)	1.99(3)	1
O(1)	2a	0	0	0	3.7(3)	0.407(8)
O(2)	4e	0	0	0.1952(2)	3.19(6)	1
O(3)	8g	0	1/2	0.0893(1)	2.85(5)	0.934(5)

R_{wp}=13%, χ^2=2.1, Dw=1.09.
[a] Space group *I4/mmm*; $a=b$=3.9338(1) Å, c=20.4616(2) Å, V=316.651(2) Å^3.

Table 3
Bond distances of $Sr_3Fe_2O_{6+\delta}$ at various T in the range $20 \le T \le 900$ °C

	20 °C	300 °C	500 °C	700 °C	900 °C
Sr(1)–O(1)×4	2.732(1)	2.743(1)	2.754(1)	2.767(1)	2.782(1)
Sr(1)–O(3)×8	2.685(1)	2.698(1)	2.694(1)	2.686(1)	2.685(1)
Sr(2)–O(2)×4	2.742(1)	2.753(1)	2.765(1)	2.779(1)	2.794(1)
Sr(2)–O(2)×1	2.488(4)	2.499(4)	2.497(6)	2.493(6)	2.501(6)
Sr(2)–O(3)×4	2.648(3)	2.654(3)	2.683(4)	2.716(4)	2.739(4)
Fe–O(1)	1.987(2)	1.995(2)	2.023(2)	2.050(2)	2.068(2)
Fe–O(2)	1.921(4)	1.931(4)	1.928(4)	1.927(4)	1.927(4)
Fe–O(3)	1.936(1)	1.943(1)	1.954(1)	1.968(1)	1.982(1)

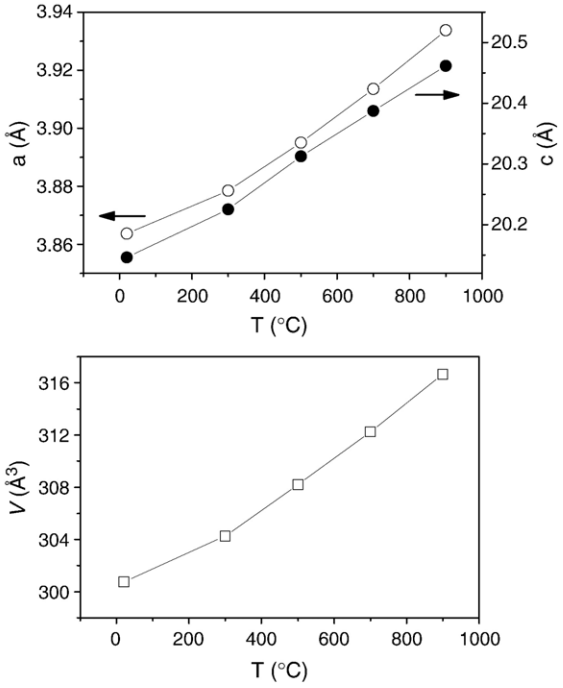

Fig. 3. Variation of the lattice parameters a and c and the unit cell volume V with temperature.

agreement with the total oxygen content determined by iodometric titration, 6.76(1) [26], and thermogravimetric analysis under hydrogen, 6.75(5) [15] for samples of $Sr_3Fe_2O_{6+\delta}$ prepared under similar conditions. On one hand, the oxygen vacancies were located mainly on the O(1) (2a, 0, 0, 0) site connecting the octahedra along the c axis in agreement with previous data at room temperature for $Sr_3Fe_2O_{6+\delta}$ [15] and $Sr_3FeCoO_{6+\delta}$ [20]. On the other hand, the O(2) (4e, 0, 0, z) site located in the rock salt layer was fully occupied at all the temperatures. However, our results also indicate the presence of a nonnegligible concentration of oxygen vacancies on the O(3) (8g, 0, 1/2, z) site in the FeO_2 planes of the perovskite layers when the oxygen content is above 6.0. The quality of the refinement diminishes when the model assumes the full occupancy of the O(3) site and oxygen vacancies only on the O(1) site. For example, at T=900 °C the factors R_{wp} and χ^2 raise from the values 13 and 2.1 to the values 13.7 and 2.32, respectively. The occupancies obtained for O(1) and O(3) at each temperature were the same within the estimated standard deviation for each set of initial values used to overcome correlation effects between thermal and occupancy parameters. Fig. 4b and c shows the variations with temperature of the oxygen occupancy on the O(1) and O(3) sites, respectively. The oxygen occupancy, and therefore the oxygen content associated to each crystal site, decreases continuously as the temperature increases. At T=900 °C the vacancies on the O(3) site are 6.6% of the oxygen sites in the FeO_2 planes and ~0.25 per formula unit while the vacancies on the O(1) site account for 60% of these sites and ~0.6 per formula unit. The presence of oxygen vacancies on the O(3) site was reported for the n=2 R–P phases $Sr_3FeCoO_{7-\delta}$ with δ=1.55 and 1.1 [20] and $Sr_3Co_2O_{5+\delta}$ with δ=0.91, 0.64 and 0.38 [27]. In this case, the samples were quenched to room temperature after the appropriate heat treatment to obtain oxygen contents below 6.0 [20,27]. Other studies inferred the presence of oxygen vacancies on the O(3) site when the oxygen content is above 6.0 after analyzing thermodynamic [16] and ionic conductivity data [17]. We have recently reported thermodynamic data of $Sr_3Fe_2O_{6+\delta}$ at high temperature where the variation of the partial molar entropy (sO_2) with the oxygen content was reproduced with a simple defect model. This model was based on the mass action law assuming localized charge carriers and random oxygen

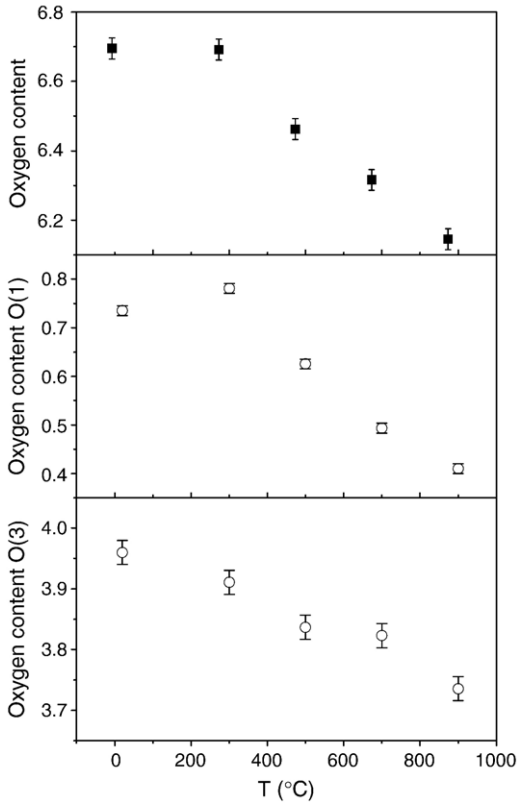

Fig. 4. Variation of the oxygen content per formula unit with temperature, in air: a) total oxygen content, b) O(1) (2a, 0, 0, 0) site and c) O(3) (2g, 0, 1/2, z) site.

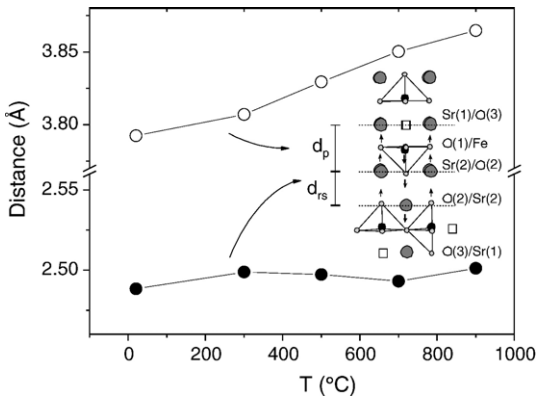

Fig. 5. Variation of the width of the perovskite and rock salt layers with temperature in the crystal structure of $Sr_3Fe_2O_{6+\delta}$. The inset shows a portion of the crystal structure describing both the perovskite and the rock salt layers and the displacements of the atoms with respect to the Sr(1)/O(1) plane.

vacancies located on the O(1) and O(3) sites. Moreover, the presence of vacancies on the O(3) position is also in agreement with the pathways suggested by Shilova et al. [17] for oxygen ion migration in this compound.

The Fe–O coordination polyhedra changes from octahedra to pyramids as the oxygen atoms are removed from the crystal structure [20]. The Fe–O bond lengths at room temperature listed in Table 3 show an excellent agreement with the values reported for $Sr_3Fe_2O_{6.75}$ in Ref. [15]. After the removal of the oxygen atom from the O(1) position, this crystal site behaves like a positive charge causing the relaxation of the surrounding ions. Thus the Fe cations move outward on the *c* direction, while the O(3) oxygen ions move towards the oxygen vacancy. These relative displacements result in a Fe cation that resides above the equatorial plane of the FeO_6 octahedra. This displacement may also be the origin for the negative chemical expansion of the lattice parameter *c* discussed above. The displacement of the oxygen atoms O(3) causes the expansion of the bond length Sr(2)–O(3), while the Sr(1)–O(3) distance remains almost constant. Furthermore, the distance Sr(2)–O(2) along the *c* axis in the rock salt layer shows little variation with temperature. Thereby, it is mainly the perovskite block which absorbs the expansion along the *c* axis. This effect is shown in Fig. 5 where the width of the perovskite layer (d_p) is measured from the plane Sr(1)/O(1) to the plane Sr(2)/O(2), while the width of the rock salt layer (d_{rs}) defined between two planes Sr (2)/O(2) remains constant.

The crystal chemistry of $Sr_3Fe_2O_{6+\delta}$ at high temperature is important for a better understanding of the oxide-ion diffusion mechanism in this mixed conductor. In the case of perovskite oxides with large oxygen deficiency, the oxygen ion diffusion occurs by an anion vacancy mechanism usually between equivalent crystal sites. The formation and migration of interstitial oxygen ions is usually unfavorable to occur [28], although it was found to be the mechanism for oxygen migration in the R–P phase $La_2NiO_{4+\delta}$ [29,30] that contains oxygen atoms in excess ($\delta>0$). The large oxygen non-stoichiometry of the $Sr_3Fe_2O_{6+\delta}$ compound localized in the perovskite block, and the diminution of σ_i with the reduction of the oxygen vacancy concentration due to the replacement of $Fe^{3+/4+}$ for Ti^{4+} [17] are the main evidences to assume that a vacancy mechanism occurs in this material. Shilova et al. [17] suggested that even if the oxygen vacancies were located only on the O(1) site, oxygen ion diffusion should involve the ion jumps from the O(3) to the O(1) site along the FeO_6 octahedron edge like in the perovskite phases [28]. The experimental evidence obtained in this work indicating the presence of oxygen vacancies in the FeO_2 plane reinforces this view. Although the O(1) and O(3) sites are not energetically equivalent, we speculate that the difference of the ion potential energies have to be little to explain the simultaneous presence of oxygen vacancies at both crystal sites at high temperature. At the same time it makes feasible the oxygen ion migration from the O(3) to the O(1) site. Besides, the presence of structural oxygen vacancies on the O(3) site suggests an alternative pathway for oxygen diffusion involving only O(3) sites. The distance $d_{O(3)–O(3')}$= 2.782 Å calculated from NPD data at T=900 °C is smaller than the distance $d_{O(3)–O(1)}$=2.854 Å. These two distances are obviously smaller than the distance $d_{O(1)–O(1')}$=3.934 Å needed to jump from the O(1) position to a nearby O(1′) site. The ionic conductivity σ_i is proportional to the square of the jump distance and to the concentration of ions diffusing, which results in a variation inversely proportional to the jump distance [31]. Thereby we expect that the main contribution to σ_i comes from oxygen ions using O(3)–O(1) and O(3)–O(3′) jumps.

4. Conclusions

The oxygen defect structure of the n=2 Ruddlesden–Popper phase $Sr_3Fe_2O_{6+\delta}$ has been determined through the analysis of *in situ* high temperature NPD in the temperature range $20 \le T \le 900$ °C in air. The refinement of NPD data reveals the presence of a nonnegligible concentration of oxygen vacancies on the O(3) sites in the FeO_2 planes of the perovskite layers along with the oxygen vacancies located on the O(1) sites linking the octahedra between perovskite layers. The localization of the oxygen vacancies on the O(3) position is a strong evidence to understand the pathways for the oxygen ion migration mechanism that should include jumps from the position O(3) to either a neighboring empty O(3′) site within the FeO_2 plane or a nearby empty O(1) site. Also, the finding of oxygen vacancies on the O(3) position supports the defect model based on the mass action law with localized charge carriers and random oxygen vacancies located at the O(1) and O(3) sites proposed to reproduce thermodynamic data of $Sr_3Fe_2O_{6+\delta}$ [16].

From the analysis of the variation of bond distances with temperature, we found that the total expansion along the *c* axis $\alpha_c = 17.7(5)\cdot 10^{-6}$ K^{-1} mainly affects the perovskite block while the width of the rock salt layers remains stable. The value of the volumetric total expansion $\alpha_V/3 = 20(1)\cdot 10^{-6}$ K^{-1} is comparable to the average of the linear total expansion reported for the perovskite system $La_{1-x}Sr_xCo_{1-y}Fe_yO_{3-\delta}$ with $0 \le y \le 1$ and $0 \le x \le 1$.

Acknowledgments

This work was supported by CNEA (Argentine Atomic Energy Commission), CONICET (Argentine Research Council), through PIP 5594, Fundación Antorchas (Argentina), ANPCyT through PICT 02–12–12455 and PICT 03–12–14493 and Cooperation Program ECOS-SUD.

References

[1] H.J.M. Bouwmeester, A.J. Burggraaf, in: P.J. Gellings, H.J.M. Bouwmeester (Eds.), The CRC Handbook of Solid State Electrochemistry, CRC Press, Boca Raton, FL, 1997 (Chapter 14).
[2] S.J. Skinner, Int. J. Inorg. Mater. 3 (2001) 113–121.
[3] E.A. Hazbun, U.S. Patent 4,791,079, 1988; E.A. Hazbun, U.S. Patent 4,827,071, 1989.
[4] Y. Teraoka, H.M. Zhang, S. Furukawa, N. Yamazoe, Chem. Lett. (1985) 1743–1746.
[5] Y. Teraoka, H.M. Zhang, K. Okamoto, N. Yamazoe, Mates. Res. Bull 23 (1988) 51–58.
[6] L.M. Liu, T.H. Lee, L. Qiu, Y.L. Yang, A.J. Jacobson, Mater. Res. Bull 31 (1996) 29–35.

[7] N. Grunbaum, L. Mogni, F. Prado, A. Caneiro, J. Solid State Chem 177 (2004) 2350–2357.
[8] F. Prado, N. Grunbaum, A. Caneiro, A. Manthiram, Solid State Ionics 167 (2004) 147–154.
[9] S. McIntosh, J.F. Vente, W.G. Haije, D.H.A. Blank, H.J.M. Bouwmeester, Solid State Ionics 177 (2006) 833–842.
[10] S.N. Ruddlesden, P. Popper, Acta Crystallogr. 11 (1958) 54–55.
[11] A. Manthiram, F. Prado, T. Armstrong, Solid State Ionics 152–153 (2002) 647–655.
[12] F. Prado, T. Armstrong, A. Caneiro, A. Manthiram, J. Electrochem. Soc. 148 (2001) J7–J14.
[13] T. Armstrong, F. Prado, A. Manthiram, Solid State Ionics 140 (2001) 89–96.
[14] K.T. Lee, A. Manthiram, Chem. Mater. 18 (2006) 1621–1626.
[15] S.E. Dann, M.T. Weller, D.B. Currie, J. Solid State Chem 97 (1992) 179–185.
[16] L. Mogni, J. Fouletier, F. Prado, A. Caneiro, J. Solid State Chem 178 (2005) 2715–2723.
[17] Y.A. Shilova, M.V. Patrakeev, E.B. Mitberg, I.A. Leonidov, V.L. Kozhevnikov, K.R. Poeppelmeier, J. Solid State Chem 168 (2002) 275–283.
[18] L. Mogni, F. Prado, A. Caneiro, A. Manthiram, Solid State Ionics 177 (2006) 1807–1810.
[19] L. Mogni, F. Prado, A. Caneiro, Chem. Mater. 18 (2006) 4163–4170.
[20] Y. Bread, C. Michel, F. Hervieu, Studer, A. Maignan, B. Raveau, Chem. Mater. 14 (2002) 3128–3135.
[21] M. Matvejeff, M. Lehtimäki, A. Hirasa, Y.-H. Huang, H. Yamauchi, M. Karppinen, Chem. Mater. 17 (2005) 2775–2779.
[22] J. Rodríguez-Carvajal, Fullprof: a program for Rietveld refinement and profile matching analysis of complex powder diffraction patterns, Laboratoire Léon Brillouin (CEA-CNRS), France, 2002.
[23] P. Thompson, D.E. Cox, J.B. Hastings, J. Appl. Cryst 20 (1987) 79–83.
[24] K.T. Lee, D.M. Bierschenk, A. Manthiram, J. Electrochem. Soc 153 (2006) A1255–A1260.
[25] A. Petric, P. Huang, F. Tietz, Solid State Ionics 135 (2000) 719–725.
[26] L. Mogni, F. Prado, H. Ascolani, M. Abbate, M.S. Moreno, A. Manthiram, A. Caneiro, J. Solid State Chem 178 (2005) 1559–1568.
[27] L. Vicio, H.W. Zandbergen, Q. Xu, Q. Huang, M. Lee, R.J. Cava, J. Solid State Chem 179 (2006) 501–512.
[28] M.S. Islam, J. Mater. Chem 10 (2000) 1027–1038.
[29] L. Minervini, R.W. Grimes, J.A. Kilner, K.E. Sickafus, J. Mater. Chem 10 (2000) 2349–2354.
[30] J.M. Bassat, P. Odier, A. Villesuzanne, C. Marin, M. Pouchard, Solid State Ionics 167 (2004) 341–347.
[31] J.B. Goodenough, Proc. R. Soc. Lond. A 393 (1984) 215–234.